FERMILAB-CONF-75-103-E #27A
COO-3065-119 #305

UR-541

STUDIES OF NEUTRON DISSOCIATION AT FERMILAB ENERGIES

BY

T. FERBEL

THE UNIVERSITY OF ROCHESTER

DEPARTMENT OF PHYSICS AND ASTRONOMY

ROCHESTER , NEW YORK

UR-541 COO-3065-119

STUDIES OF NEUTRON DISSOCIATION AT FERMILAB ENERGIES*

T. Ferbel

University of Rochester+, Rochester, New York 14627

June 20, 1975

In this report I will summarize the latest results obtained in a continuing investigation of neutron dissociation into ($p\pi^-$) systems in neutron-nuclear collisions between 50 GeV/c and 300 GeV/c.(1) The experiment is a collaborative effort involving physicists from Fermilab, Northwestern University, University of Rochester and SLAC (see Table I).

TABLE I

Primary Contributors to Experiment

J. Biel*	L. Kenah‡
E. Bleser†	J. Rosen‡
T. Ferbel*	R. Ruchti‡
D. Freytag#	P. Slattery*
B. Gobbi‡	D. Underwood*

*University of Rochester: †Fermilab: #SLAC: ‡Northwestern University

The measurements were performed in the M-3 neutral beam of the Meson Detector Building at the Fermi National Accelerator Laboratory. A variety of nuclear targets ranging from hydrogen to uranium were employed in this

*Invited paper delivered at the Intl. Conf. on High Energy Physics at Palermo, Italy (1975).

+Research supported by the United States Energy Research and Development Administration. (Contract Number E(11-1)-3065.

study. I will first briefly discuss our nuclear coherent dissociation data; subsequently I will present new measurements of total cross sections of neutrons on nuclei in the Fermilab momentum range; finally I will report on neutron dissociation using a hydrogen target and compare the hydrogen data with expectations from simple Deck models.

DISSOCIATION USING NUCLEAR TARGETS

The apparatus, which is sketched in Fig. 1, consists of a large aperture wire-plane spark chamber V-spectrometer. The nuclear-target box is located 400 meters downstream of the neutron-beam production target. Nuclear targets, typically 0.1 radiation lengths in thickness, were used to study coherent production of $p\pi^-$ systems. The target box was surrounded with scintillator/lead sandwich veto counters so as to detect nuclear break up processes and thus reduce the trigger level for the experiment. The trigger requirements were designed to suppress incoherent production as well as the production of more than two charged particles within the target box. Specifically, the logic condition $\bar{A}\cdot S\cdot H1$ was required to be satisfied for an acceptable trigger. Here, A represents the logical OR of all the veto counters, i.e. the counters surrounding the target box, the $\frac{1}{16}$ inch thick scintillation veto counter at the entry to the target box (indicating that the particle initiating the collision was charged rather than neutral), and the various baffle counters surrounding the magnet aperture (indicating presence of charged or neutral particles in addition to those entering the magnetic field volume); S represents a $\frac{1}{32}$ inch scintillation trigger counter located 2 inches downstream of the nuclear target sample. Two and only two of the six H1 hodoscope elements (immediately downstream of the magnet) were required to have signals before the acceptance requirement was fulfilled. The spark chambers were capable

of being pulsed 15 times during the ~1 sec beam spill. A typical run consisted of 10,000 triggers taken over a six hour period. Quality of the performance of the apparatus was monitored using an online PDP-15 DEC computer; reconstruction of events and analysis was performed off-line. Approximately 80% of the 600,000 triggers yielded successfully reconstructed events.

The coherent dissociation of neutrons can proceed either through the hadronic diffractive dissociation[2] process (often referred to as Pomeranchukon exchange) or through the electromagnetic excitation of the neutron in the coulomb field of the target nucleus (Primakoff effect, or photon exchange).[3] The dissociation of neutrons has been studied at lower energies,[4] where kinematic restrictions cause a severe suppression of the coherent cross section, particularly at large values of $p\pi^-$ mass (M). In this report I will present the general characteristics of the $p\pi^-$ mass spectra and the momentum-transfer distributions obtained in the coherent dissociation of $n \to p\pi^-$ for Pb, Cu, C and Be targets in the 120 GeV/c - 300 GeV/c momentum band.

Figure 2 displays distributions of the square of the four-momentum transfer (t) between the incident neutron and the produced $p\pi^-$ systems for three regions of M: (1) The $\Delta(1236)$ mass region, defined as $M<1.28$ GeV; (2) The $N^*(1400)$ region, defined as $1.35<M<1.45$ GeV; and (3) The $N^*(1688)$ region, defined as $1.55<M<1.80$ GeV. (We use the variable $t'=|t-t_0|$, where t_0 is the kinematically allowed minimum value of t for the production of a $p\pi^-$ system having mass M at a given value of the incident momentum for the neutron.) Corrections for target-empty measurements and for small variations in the geometrical acceptance of the apparatus have been calculated using a Monte Carlo program and were applied to the data. The steep peaks observed at small t', with values of diffractive slopes

characteristic of the sizes of the nuclear targets, give us full confidence that the inelastic production process takes place coherently over the entire nucleus. (It should be recalled that we do not measure the momentum of the recoil nucleus and consequently the reaction $n+A\rightarrow(p\pi^-)+A'$ has no constraints. We believe, however, that background from other coherent or incoherent channels is not important for the data which we present in this paper.[5])

The distributions in t', for each target, appear to show similar dependences on M. Namely, for the $\Delta(1236)$ region all the distributions display a sharpening of the t' spectrum at $t'\lesssim 0.001$ GeV^2. This excess contribution can be attributed to coulomb production of $p\pi^-$ systems, which because of the known large $\Delta n\gamma$ coupling is dominated by $\Delta^\circ(1236)$ production. Taking our experimental resolution into account, the initial fall off of the cross section in t' is consistent with the theoretically expected form for coulomb production.[6]

The smooth curves drawn on the figure are superpositions of the contributions from coulomb[6] and from diffractive coherent production. The latter is based on an optical model description for the production process described by Kolbig and Margolis.[8] Standard Woods-Saxon parameters were used to describe the nuclear shapes.[9] The total cross section of a neutron on a nucleon was taken to be a constant 39mb and the elastic forward scattering amplitude for n-nucleon and $(p\pi^-)$-nucleon was taken to be imaginary. Our experimental resolution was folded into the overall prediction for the shape of the t' spectrum. The value for the $(p\pi^-)$-nucleon total cross section was also taken to be 39mb, a value consistent with the shape observed for the t' distribution and consistent with similar measurements made at incident neutron momenta of ~12 GeV/c.[4]

Figure 3 displays the M spectra for two regions of t':

(1) $t'<0.001$ GeV^2, a region where coulomb production is important; and (2) $0.005<t'<0.03$ GeV^2, where diffractive production dominates. The data in Fig. 3 indicate substantial $\Delta(1236)$ production, particularly at small t'; a shoulder is evident at the $N^*(1520)$ and a small enhancement is observed at the $N^*(1688)$, both mainly at the larger t' values. The difference in the various M-spectra can be attributed largely to the known dependence of the coulomb production process on t' and Z (the nuclear charge). The cross section for $\Delta^\circ(1236)$ production, in particular, is approximately proportional to Z^2 for $t'<0.001$ GeV^2. The curve superimposed on the Pb data is the predicted shape of the mass spectrum expected on the basis of coulomb production. (The absolute normalization is also consistent with the data.) The curve displayed on the Be data is based on a calculation of the reggeized Deck effect.[10] The shape of the predicted mass distribution is in reasonable agreement with the data.

We have used the dominance of the coulomb cross section for production on Pb to extract the momentum spectrum of the incident neutron beam. The observed $p\pi^-$ momentum spectrum in Pb for $M<1.28$ and $t'<0.001$ was first corrected for diffractive event background. The subsequent unfolding of the resolution and of the known coulomb production process[6] provided the corrected momentum spectrum, (Fig. 4) which is consistent with the directly measured neutron spectrum using calorimetry.[7]

The energy dependence of the cross section for several mass intervals for Be, C, Cu and Pb targets is displayed in Fig. 5. Only Pb appears to show an increase of the cross section with momentum. This rise is consistent with the dominance of the coulomb process in Pb (even for large M-values). The cross sections for production using the other elements are constant to within 10% possible systematic uncertainties.

NEUTRON-NUCLEAR TOTAL CROSS SECTIONS

The cross section for neutron dissociation into $p\pi^-$ systems on Pb is ~1% of the total n-Pb cross section. Therefore, our V spectrometer can be considered as a neutron detector having excellent positional and energy resolution. We have utilized this aspect of the spectrometer to perform a precision measurement (limited only by statistics) of neutron-nuclear total cross sections. Using nuclear transmission targets located ~200 meters upstream of the spectrometer Pb target, we measured cross sections as a function of momentum. The transmission targets were cycled automatically, typically every ten minutes (a target empty position was included in the cycling). Counter telescopes were used to monitor the neutron flux throughout the data taking. Small (<0.5%) corrections for elastic scattering of the neutrons in the transmission target were also measured and applied to the data.

In Fig. 6 we display our measurements of the total cross sections of neutrons on C, Al, Cu and Pb targets as a function of beam momentum. These measurements connect up very smoothly with measurements at lower energies but appear to be somewhat inconsistent with other recent measurements at Fermilab.[11]

DIFFRACTIVE PRODUCTION ON HYDROGEN

I will now discuss our results pertaining to neutron dissociation from hydrogen in the 50 GeV/c to 300 GeV/c momentum range, the specific reaction is:

$$n + p \rightarrow (p\pi^-) + p \qquad (1)$$

The apparatus, except for the substitution of a hydrogen target for the nuclear-sample target box, is identical to that already described. The hydrogen target consists of a high-pressure vessel capable of withstanding

gas pressures of $\lesssim$100 atmospheres. The active target region is 20 inches in length; this region is defined by a thin veto-counter at the upstream end, and by a trigger counter at the downstream end of the high-pressure volume. A set of 16 plastic scintillator strips, each 1/4 inch thick, 11/16 inches wide and 20 inches long, surround azimuthally the active target region at a distance of $1\frac{3}{4}$ inches from the neutron beam axis (see Fig. 7). The sixteen scintillator elements are each viewed at both ends, with the aid of plastic light pipes, using photomultiplier tubes located outside of the high-pressure vessel.[12] The trigger requirement for an acceptable $np \rightarrow (p\pi^-)p$ event consists of the following: no signal in the upstream veto-counter contained within the target vessel, a signal in the downstream trigger counter, two and only two charged particles exiting the spectrometer magnet, and a signal in only one of the 16 azimuthal counters.

Following the spatial reconstruction of the forward $p\pi^-$ system (V) a check is made of the correlation between the transverse direction of the V system and the position of the activated azimuth counter for that event. The distribution in the angle (Φ) between the transverse direction of the forward $p\pi^-$ system and the transverse direction of the recoil proton, as specified by the center of the activated azimuthal counter, is peaked at 180° (see Fig. 7). This peak, which signifies the presence of our signal, has the expected width of ~22.5°; the peak to background ratio is ~5/1. In the data to be presented we have imposed a cut-off band on Φ centered at 180° (i.e., 180° ± 15°). To account for contamination of our $pp\pi^-$ final state, we have subtracted from the data in the signal band of Φ = 180° ± 15° the data in the sum of the background bands: Φ = 195° to 210° and Φ = 150° to 165°. A small subtraction (~2%) for target-empty was also applied to the data. The present sample of reaction (1) is

derived from a total of ~180,000 triggers of which ~60,000 passed all geometric and kinematic acceptance criteria. The largest background is from neutron dissociation into ($p\pi^-\pi^0$) systems. We believe this source of background to be at a level of ≤10% of the ($p\pi^-$) signal. (Background from ($n\pi^+\pi^-$) systems is greatly suppressed by removing events in which a neutron signal is detected in a small calorimeter downstream of the apparatus. The calorimeter subtends an angle of about ±2 mrad.)

Figure 8 displays the mass spectrum of the forward-produced $p\pi^-$ system in reaction (1), corrected for acceptance of the spectrometer. Data are shown for three t' intervals: (a) 0.02 to 0.08 GeV^2, (b) 0.08 to 0.20 GeV^2, and (c) 0.20 to 1.0 GeV^2. (The cut-off at $t' \simeq t = 0.02$ GeV^2 was chosen to assure an unbiased sample of events. The losses below $t \simeq 0.015$ GeV^2 are quite severe because, under our typical running conditions of 50 atmospheres of pressure for the hydrogen gas target, recoil protons do not have sufficient energy to reach one of the azimuthal counters to trigger the interaction.) Ignoring the contribution from coulomb production in the nuclear data, we note that the mass spectrum for $t' < 0.08$ GeV^2 is similar to those observed for nuclear targets. All mass distributions appear to display fine structure at ~1.7 GeV mass values and possible rapid changes near 1.5 GeV. Cross sections for the 1.7 GeV enhancement are more prominent at larger momentum transfers.

To investigate in more detail the correlation between t' and M for production in hydrogen we display in Fig. 9 the cross section in t' for various regions of M. A strong dependence on M is observed for the t' spectrum, particularly for M<1.4 GeV.[13] In Table II we display the results of fits of the form $\exp(-bt')$ to the data at $0.04 < t' < 0.16$ GeV^2. It is observed that the t' spectra have strong curvature (or "breaks") near $t' \simeq 0.2$ GeV^2 at small M values. For $t' > 0.4$ GeV^2 the data appear to

take on a universal form [~exp(-4.5t')], essentially independent of M. The change of slope near $t' \simeq 0.2$ GeV^2, and the disappearance of this effect at large M, has been interpreted in terms of the dominance of non-flip amplitudes for $M \lesssim 1.4$ GeV and spin-flip contributions for $M > 1.4$ GeV.[14] As will be discussed in the following sections our data indicate the presence of large flip as well as non-flip helicity amplitudes for $M < 1.4$ GeV.

To demonstrate the richness of the angular distributions we present in Fig. 10 a scatter plot of the $\cos\theta$ vs ϕ decay angles of the proton in the Gottfried-Jackson (GJ) frame. We note a severe depletion in the region of $\cos\theta \approx 0.6$ and $\phi \approx 0°$. It is interesting that a suppression of a similar nature is expected in this region of $(\cos\theta, \phi)$ space if production is dominated by the π-exchange Deck mechanism (see Fig. 11 for the Deck diagram in question).[10] In fact, as will be shown, the low-order decay moments in the Gottfried-Jackson frame display a mass dependence which can be reproduced by the Deck model.

The fact that the contribution from Deck processes is expected to peak near $\cos\theta \simeq +1$ has prompted a group at the ISR to examine the dependence of the diffractively produced two-body mass on $\cos\theta$.[15] As displayed previously in Fig. 8, at Fermilab energies there does not appear to be as dramatic a dependence of the $p\pi^-$ mass on $\cos\theta$ as was observed at the ISR. In Fig. (12) we present t distributions for $M < 1.35$ GeV, separately for negative and for positive values of $\cos\theta$. The distributions are observed to display a strong dependence on $\cos\theta$, qualitatively similar to that expected from a Deck model.

If the Deck effect contributes to our reaction, it is expected that the azimuth ϕ_H of the proton in the helicity frame of the $p\pi^-$ system will be particularly useful in distinguishing the Deck contribution from

other (perhaps resonant) production channels.[16] In Fig. (13) we display distributions in $p\pi^-$ mass for the proton's $\cos\phi_H>0.9$ and $\cos\phi_H<-0.9$ (the non-resonant π-exchange Deck contribution occurs mainly for $\cos\phi_H<0$). A clear difference is apparent between the two mass spectra, particularly at large M. A possible conclusion one may draw from these data is that two separate production processes contribute to reaction (1).

In Fig. (14) we present the energy dependence of the cross section for $p\pi^-$ production at small M (integrated over t). We observe that just as in the case of production from nuclear targets, the cross sections are energy independent between 50 and 300 GeV/c. Consequently, it appears that the gross properties of reaction (1) for low M-values are those expected for a diffractive production process of the kind indicated in Fig. 11.

COMPARISON WITH DECK MODEL

I will now present the decay angular distributions of the $(p\pi^-)$ system in order to compare our data at small M with the Deck-production model indicated in Fig. 11. The square of a simple Deck-type matrix element can be written as

$$|M|^2 \approx \left[-t_1 e^{2(t_1-\mu^2)}\right] \frac{[\frac{1}{2}(s_{\pi p}-u_1)]^{2\alpha_\pi}}{\alpha_\pi^2} (s_2-u_2)^2 \, e^{10t}, \qquad (2)$$

where t_1 and t are four-momentum transfers squared; $s_{\pi p}$ and s_2 are squares of the πp invariant masses as indicated in Fig. 11; u_1 and u_2 are respectively the squares of the four-momentum transferred to the pion from the incident neutron and target proton; $\alpha_\pi=0.9(t_1-\mu^2)$ is the pion Regge trajectory, and μ is the pion mass. The π^-p elastic differential cross section is taken proportional to exp(10t). The decay moments of the

($p\pi^-$) system were extracted by numerical integration of the above expression. In addition, a variant of the Deck model was examined. This variant consisted of expression (2) but with the first bracketed omitted. This can be regarded as a Deck model with additional absorption.

Figure 15 displays the normalized low-order moments $\langle Y_{\ell m}\rangle$ versus t for fixed mass in the Gottfried-Jackson (GJ) frame and in the helicity frame. The data are in rough agreement with the trend of the Deck calculation. A similar level of agreement is available for other ($p\pi^-$) mass values. In Fig. 3 we display the variation of the same $\langle Y_{\ell m}\rangle$ versus mass at fixed t in the GJ frame. Again, the data only roughly follow the Deck calculations.

Although the predictions from expression (2) do not agree in detail with the results of reaction (1), this is not surprising in view of the fact that expression (2) can only be expected to describe the data in a rather restricted kinematic domain of reaction (1). The regime in which the π-exchange Deck mechanism is expected to dominate is characterized by small t_1 [10], large $\cos\theta_{GJ}$ [15], or as emphasized most recently, negative $\cos\phi_H$.[16] To examine whether the Deck diagram of Fig. 11 can account for the data in the region $\cos\phi_H<-0.9$ we have compared the predictions of expression (2) with our results applying this restriction on $\cos\phi_H$ to both the model and data.

The results of the comparison are displayed in Figs. 17 and 18. It is clear that in the region of expected applicability the spin structure of the Deck amplitude is in very close agreement with the data. (A similar comparison of results for $\cos\phi_H>0.9$ with a proton-exchange Deck calculation indicates a comparable level of agreement between model and data.[17] This agreement is particularly remarkable in view of the uncertainty in the origin of the M-t correlation in the data.[18]

HELICITY AMPLITUDES AT LOW MASS

The origin of the observed correlation between the mass M of an inelastic system produced in diffraction dissociation and the square of the four-momentum transferred to that system (t) has been the object of extensive investigation.[13] One attractive model for understanding the t-M interdependence in these highly peripheral reactions is based on the assumption that s-channel helicity amplitudes for small masses ($M \lesssim 1.3$ GeV) are dominantly helicity non-flip.[14] Consequently one expects a steep differential cross section for small t and a dip or sharp break near $-t \sim 0.2$-0.3 *if the helicity non-flip system is produced peripherally* (i.e., near an impact parameter b~1 Fermi). The contributions from the helicity flip amplitudes are hypothesized to become more important as the mass and spin of the diffractively produced system increases, thus leading to a substantial broadening of the t-distributions with increasing M values.[14] The $\langle Y_{11} \rangle$ moment in the helicity-frame consists of interference terms proportional to an helicity non-flip amplitude and a unit helicity-flip amplitude. In terms of the s-channel peripheral model discussed above,[14] one therefore expects $\langle Y_{11} \rangle$ in the helicity frame to pass through zero at the t value where a dip appears in the differential cross section. Similarly, one also expects a zero in $\langle Y_{11} \rangle$ near $-t \sim 0.6$ where the single helicity-flip amplitudes are predicted to have a zero. The absence of these predicted zeroes in $\langle Y_{11} \rangle$ of Fig. 15 implies that *the s-channel peripheral model cannot be the dominant production process.*

It is expected that the spin structure for $p\pi^-$ masses below ~1.5 GeV is sufficiently simple to allow an extraction of the production amplitudes. In Fig. 19 we display the preliminary results of an amplitude analysis of the data. $\langle Y_{\ell m} \rangle$ are negligible for $\ell > 4$ and (in the GJ frame) for $m > 2$. Therefore spins up to J=5/2 and helicity-flips ±1 saturate the moments.

(The $m \leq 2$ cutoff in $\langle Y_{\ell m} \rangle$ is a consequence of Pomeranchukon exchange in the s_2 subsystem of Fig. 11.) It should be recalled that there is an ambiguity in the overall sign of the amplitudes. There is also an overall ambiguity in the relative parities of all even and odd states: the amplitudes labeled S^1, D^3, F^5 can be relabeled respectively as P^1, P^3, D^5 and vice versa.

The t-channel helicity amplitudes shown in Fig. 19 indicate that both helicity flip and non-flip terms are of comparable size and of comparable degree of peripherality. In addition, the presence of large S^1 and P^3 states (or alternately P^1 and D^3 states if all parities are reversed) speaks against the validity of the Morrison selection rule in diffraction production.[19]

SUMMARY

In summary, we have examined the characteristics of diffraction dissociation of neutrons into $p\pi^-$ systems at high energies. A substantial correlation is observed between the mass and the t of the produced system. The spin structure of the $p\pi^-$ amplitudes at low mass is described surprisingly well by the simple Deck mechanism. The t-channel helicity amplitudes contain comparable contributions from flip and non-flip terms and the produced states are not restricted to those expected on the basis of the Morrison rule.

I thank J. Biel, L. Kenah and D. Underwood for providing the latest neutron dissociation data, I also thank D. Duke and P. Slattery for extensive discussions pertaining to the analysis of the results presented in this report. Finally, I wish to acknowledge helpful conversations with E. Berger and G. Fox.

REFERENCES

1. My summary is based on our three papers on neutron dissociation submitted to this conference by J. Biel et al.

2. M. L. Good and W. D. Walker, Phys. Rev. 120, 1857 (1960).

3. A. Halprin, C.M.Anderson and H. Primakoff, Phys.Rev. 152, 1295 (1966).

4. D.O'Brien et al., Nucl. Phys. B77, 1 (1974); W.Carithers et al., University of Rochester Report submitted to London Conference (1974).

5. The contribution from $n \to p\pi^-\pi^0$ dissociations, for example, which we consider to be the largest source of background, is estimated to be <15% of the $p\pi^-$ dissociations for $t' < .03$ GeV^2. Compared to the $p\pi^-$ signal events the t-dependence of this background is rather flat.

6. We have used the formulations provided by G.Fäldt, Nucl. Phys. B43, 591 (1972); C. Bemporad, et al., Nucl. Phys. B51, 1 (1973). The $\gamma n \to p\pi^-$ cross sections were obtained from the compilation of H.Genzel and W.Pfeil, Bonn Univ. PI B1-168 (1972).

7. M. Longo, et al., University of Michigan Report UM-HE-74-18 (1974).

8. K.Kolbig and B.Margolis, Nucl. Phys. B6, 85 (1968).

9. B. Hahn et al., Phys. Rev. 101, 1131 (1956); H.R.Collard et al., Landolt-Börnstein new series I/2 nuclear radii.

10. See, for example, E.L.Berger, Phys.Rev. Letters 21, 701 (1968).

11. L. Jones et al., Phys. Rev. Letters 33, 1440 (1974) and P. Murthy et al., University of Michigan Report UM HE-75-2 (1975).

12. A report describing the properties of the high-pressure gas target is in preparation.

13. See, for example, the following: J. Bartsch et al., Phys.Letters 27B, 336 (1968); B.Y.Oh and W.D.Walker, Phys. Letters 28B, 564 (1969); M.S.Farber et al., Phys. Rev. Letters 22, 1394 (1969); H.I.Miettinen and P. Pirila, Phys. Letters 40B, 127 (1972); the review of J. Rushbrooke, Proc. III Intl. Colloquium on Multiparticle Dynamics, Zakopane (1972), A. Bialas et al., eds; H. Lubatti and K.Moriyasu, Lett. Nuovo Cimento 12, 97 (1975).

14. See, for example, S. Humble, Nucl. Phys. B76, 137 (1974). For an earlier discussion of helicity flip contributions in Pomeranchukon processes see G. Kane, Acta Phys. Pol. B3, 845 (1972). See also T. Ferbel, University of Rochester Report UR-875-337 and SLAC Report 144 (1971).

15. E. Nagy et al., CERN preprint 74-1321 (June 1974). This group investigated the dissociation of the proton rather than neutron; in particular, they examined the reaction $pp \to p\pi^+$.

16. For a recent summary of the phenomenology see the excellent review of E. Berger, ANL Report ANL-HEP-PR-75-06 (1975).

17. Private communication from D. Duke.

18. For a critique of the M-t interdependence available in the Deck model see H. I. Miettinen, Proceedings of the Zakopane Colloquium (1972). A. Bialas et al., eds. For a re-examination of this question see V. A. Tsarev, Phys. Rev. D11, 1864 (1975).

19. D. R. O. Morrison, Phys. Rev. 165, 1699 (1968).

Table II

Slope Parameter Values

Mass Interval (GeV)	Slope[a] (GeV^{-2})
<1.25	19.1 ± 0.9
1.25 - 1.35	15.0 ± 0.7
1.35 - 1.45	12.8 ± 0.6
1.45 - 1.55	6.8 ± 0.7
1.55 - 1.65	4.9 ± 0.6
1.65 - 1.75	4.2 ± 0.6
1.75 - 2.00	4.2 ± 0.8

[a] Value of the parameter b from a fit of the data to the form exp(bt). The range of $|t|$ in the fit was 0.04 to 0.16 GeV^2 for the first four mass bands and .04 to 0.5 GeV^2 for the last three mass regions.

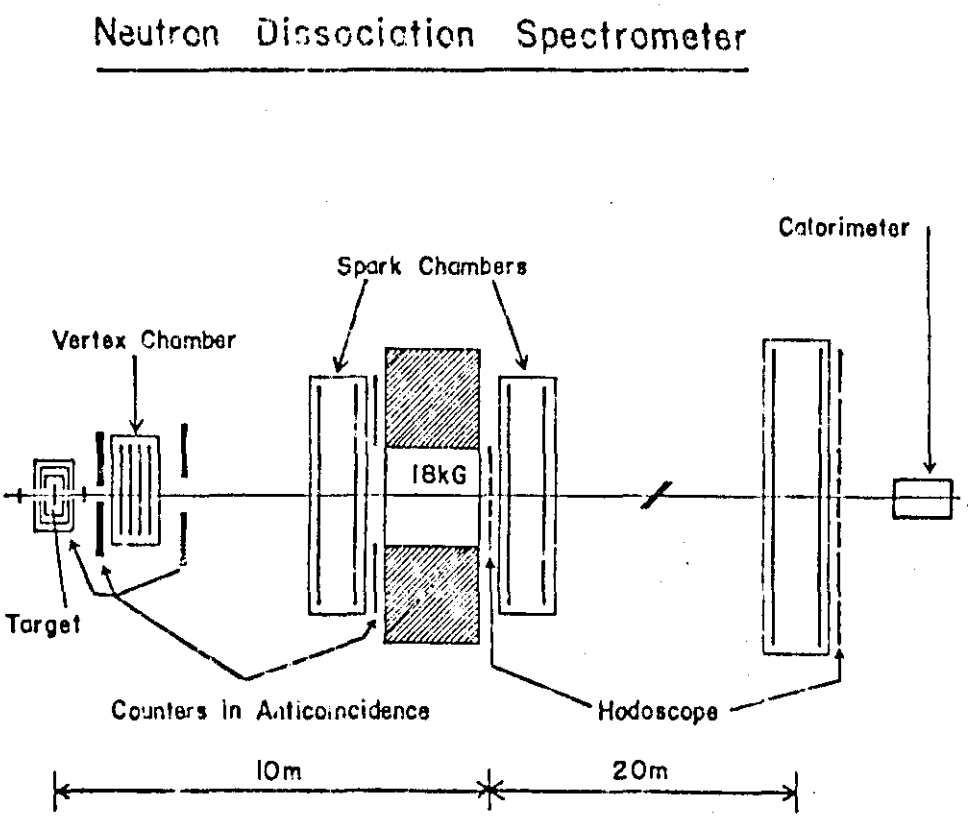

Fig. 1. Schematic of spectrometer system.

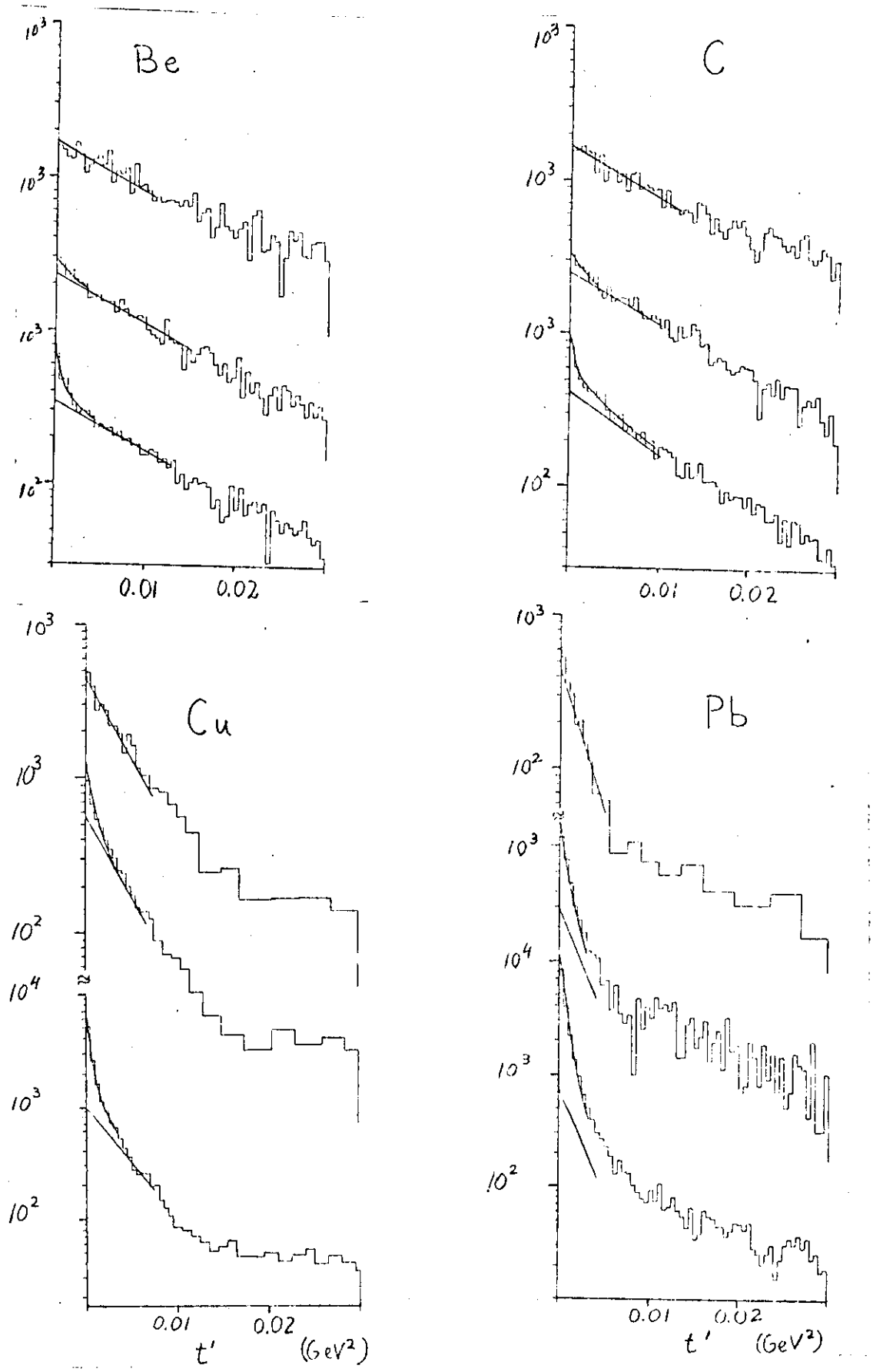

Fig. 2. Distributions in momentum transfer for neutron dissociation off Be, C, Cu and Pb nuclei. In each case we display the t spectra for $p\pi^-$ mass ranges <1.25 GeV, 1.35-1.45 GeV and 1.55-1.80 GeV (data for the lowest mass band are shown at the bottom of each set). The curves indicate the contribution of diffractive production (bottom curves) and the sum of diffractive and coulomb production (top curves).

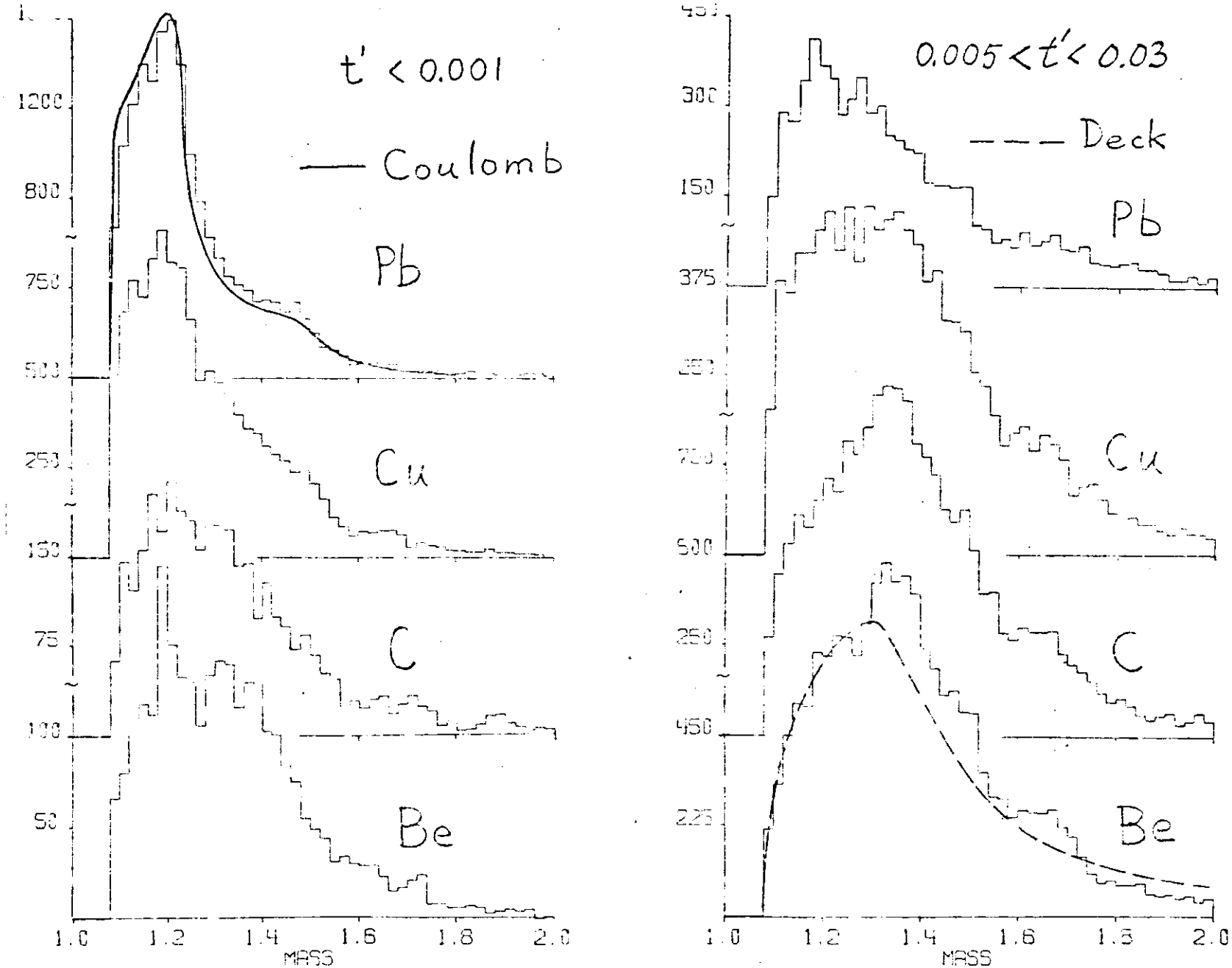

Fig. 3. Mass spectra for coherent produced $p\pi^-$ pairs for $t'<.001$ GeV^2 and $.005<t'<0.03$ GeV^2. The curve on the Pb data is the shape expected for the mass distribution assuming dominance of the Primakoff production amplitude. The curve on the Be data indicates the shape expected on the basis of a reggeized Deck model.

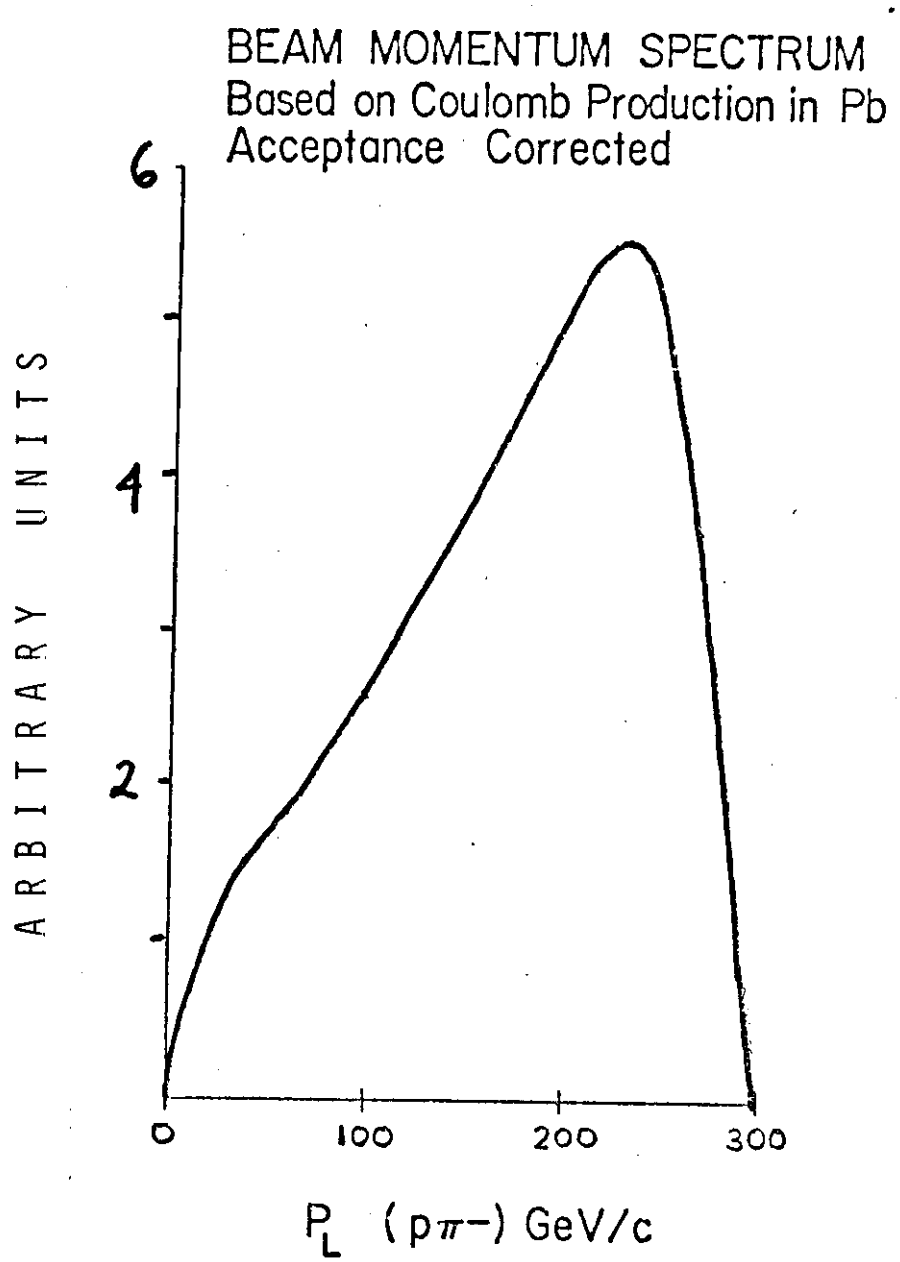

Fig. 4. Neutron momentum spectrum in the M-3 beam at Fermilab.

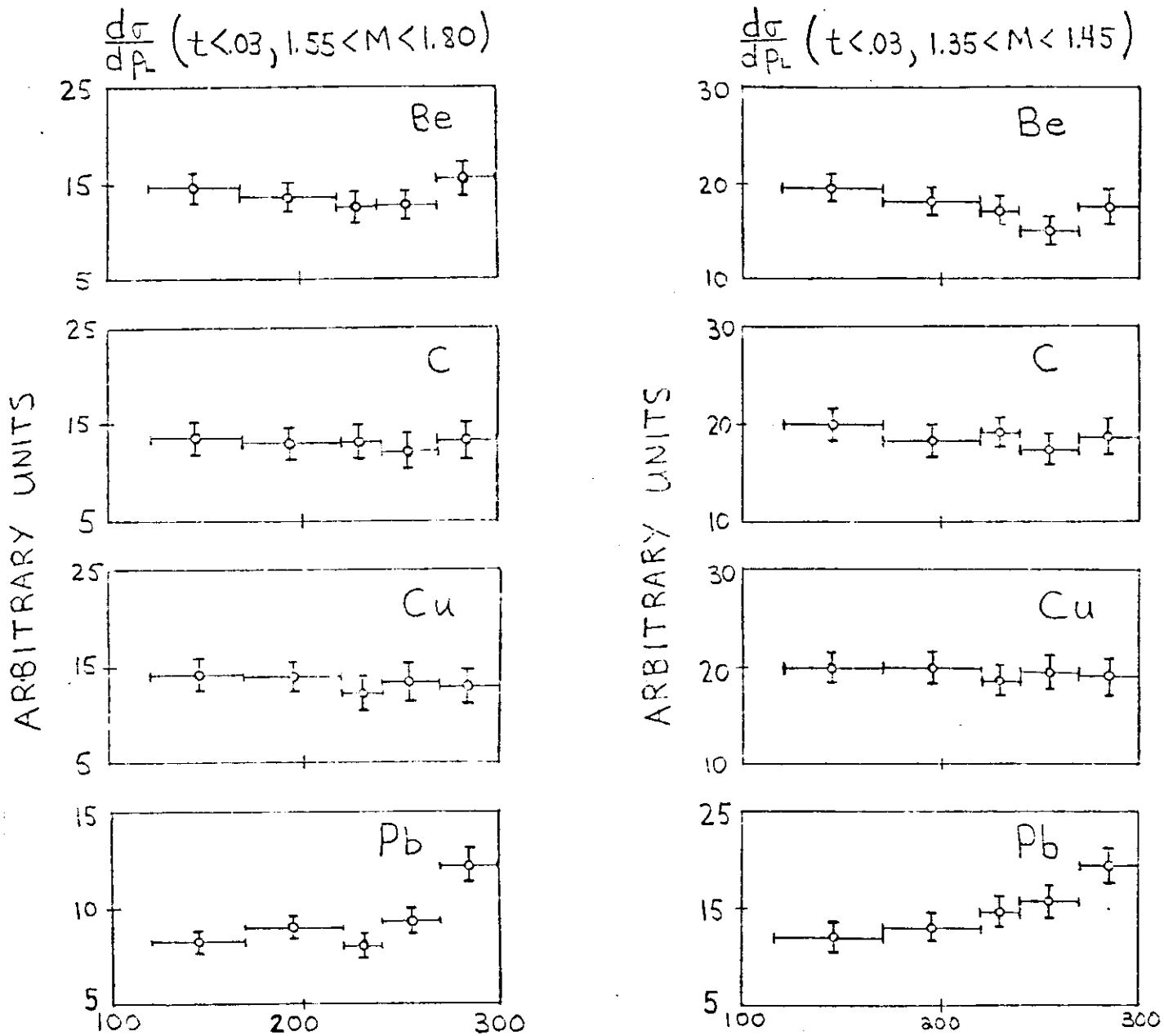

Fig. 5. Energy dependence of coherent production cross section on nuclei.

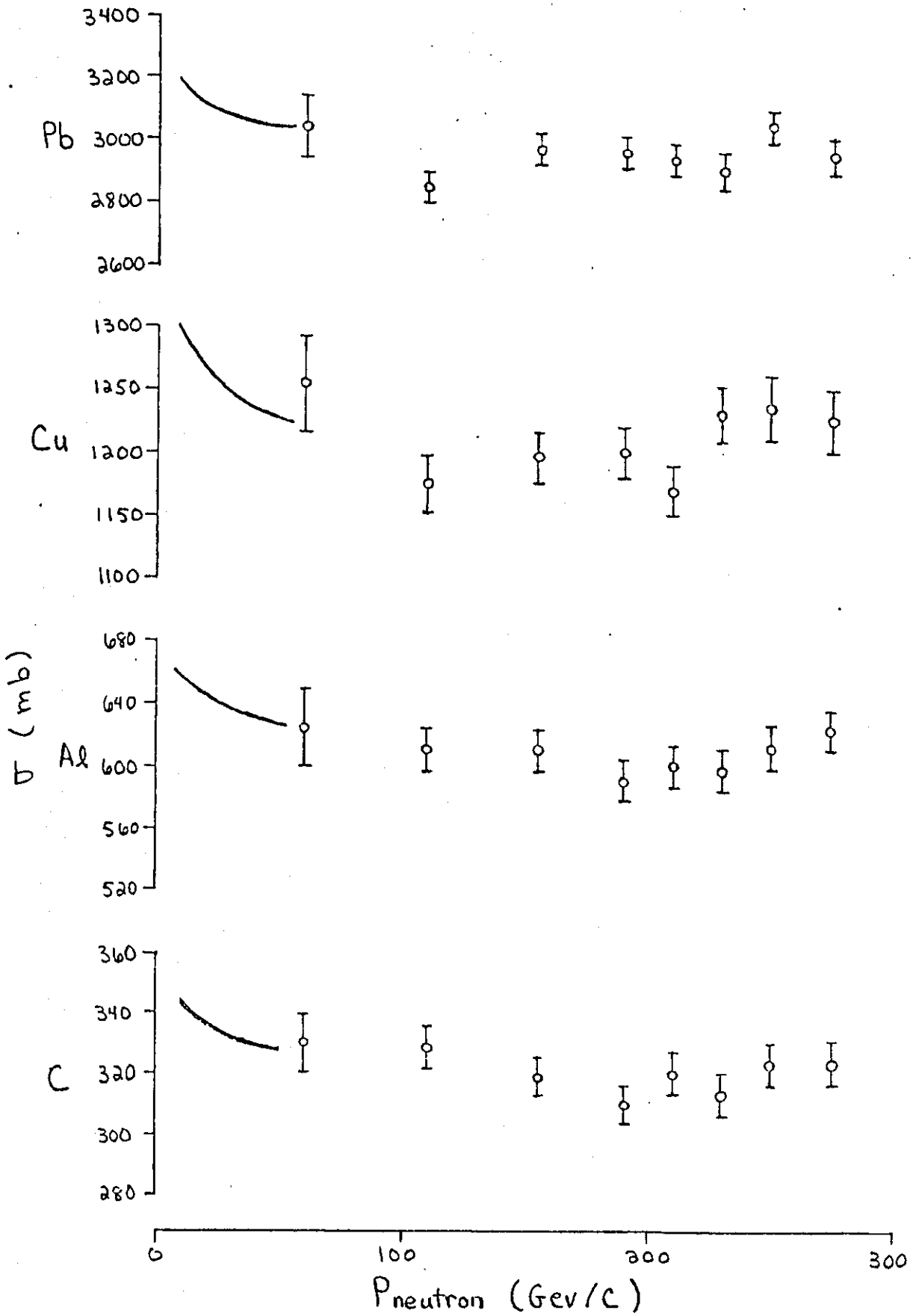

Fig. 6. Energy dependence of total neutron-nuclear cross sections. The curves indicate an averaging of measurements at lower energies.

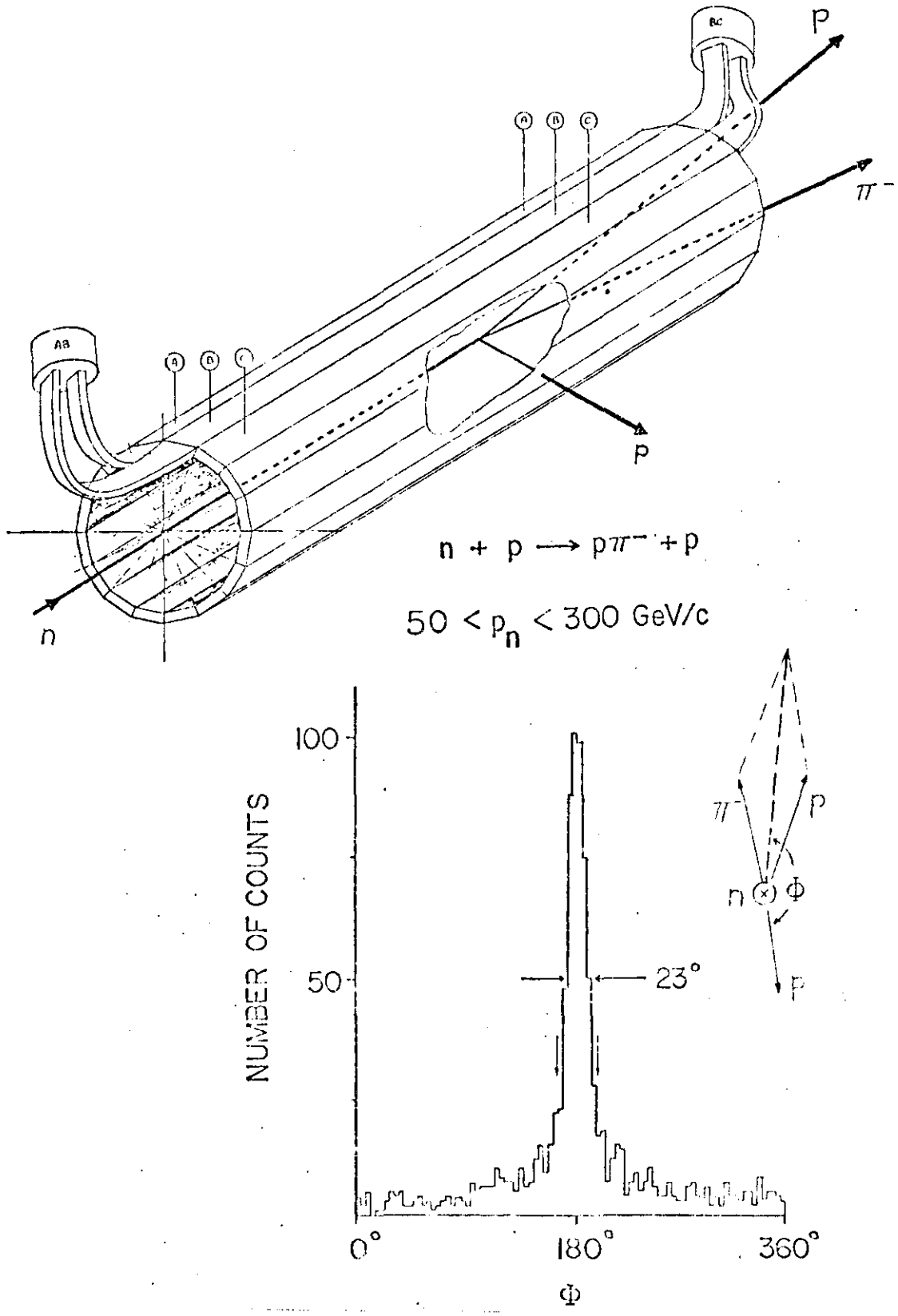

Fig. 7. Schematic of the sixteen scintillation strips placed azimuthally about the hydrogen target region. The angle Φ is between the center of an activated strip (recoil proton) and the transverse momentum of the forward produced $p\pi^-$ system (V).

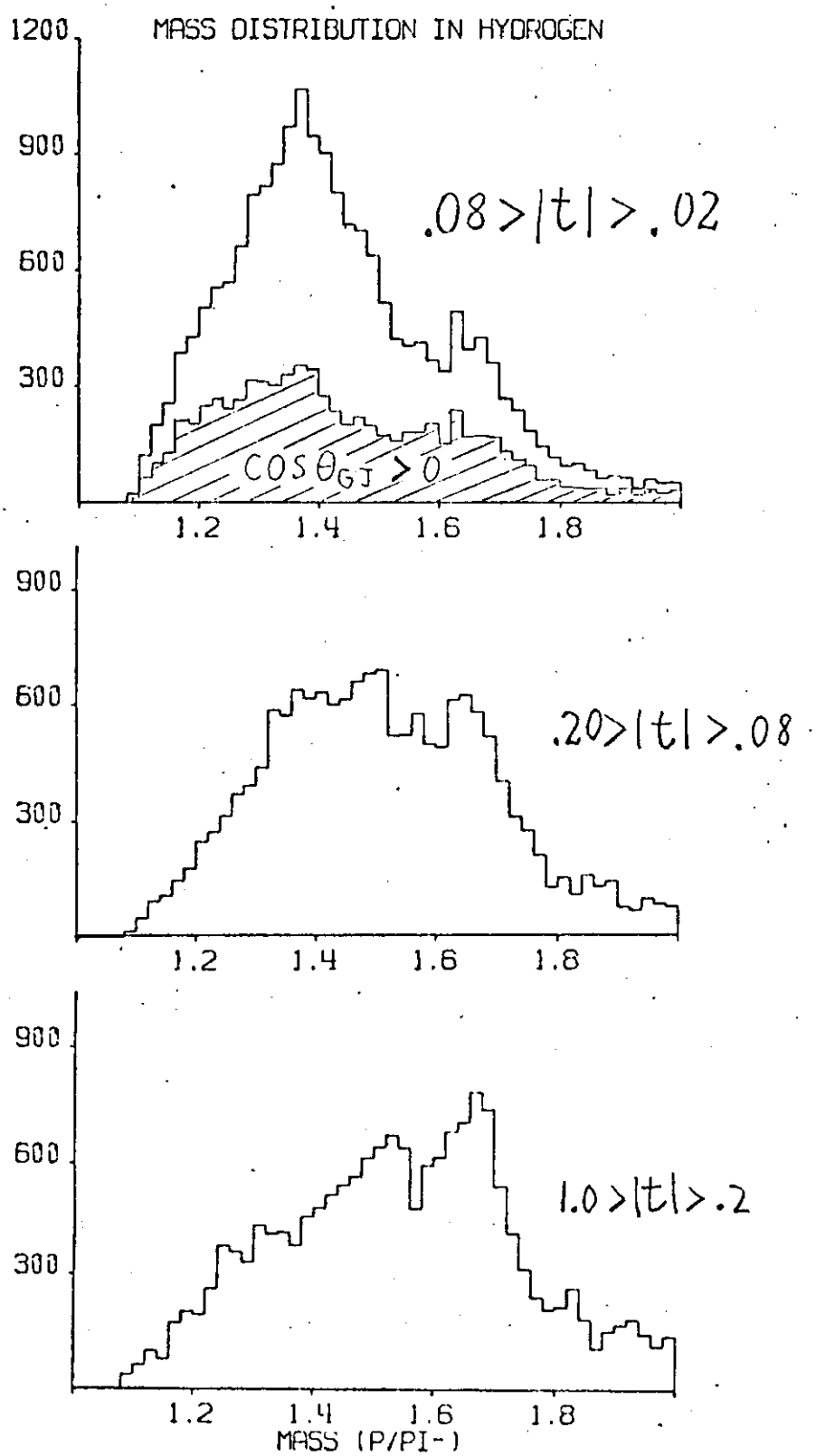

Fig. 8. Mass distribution of $p\pi^-$ systems for several regions of t. The cross hatched insert at the top corresponds to events with $\cos\theta>0$ (Gottfried-Jackson angle of the forward proton). At the larger t values there is only a weak dependence on $\cos\theta$.

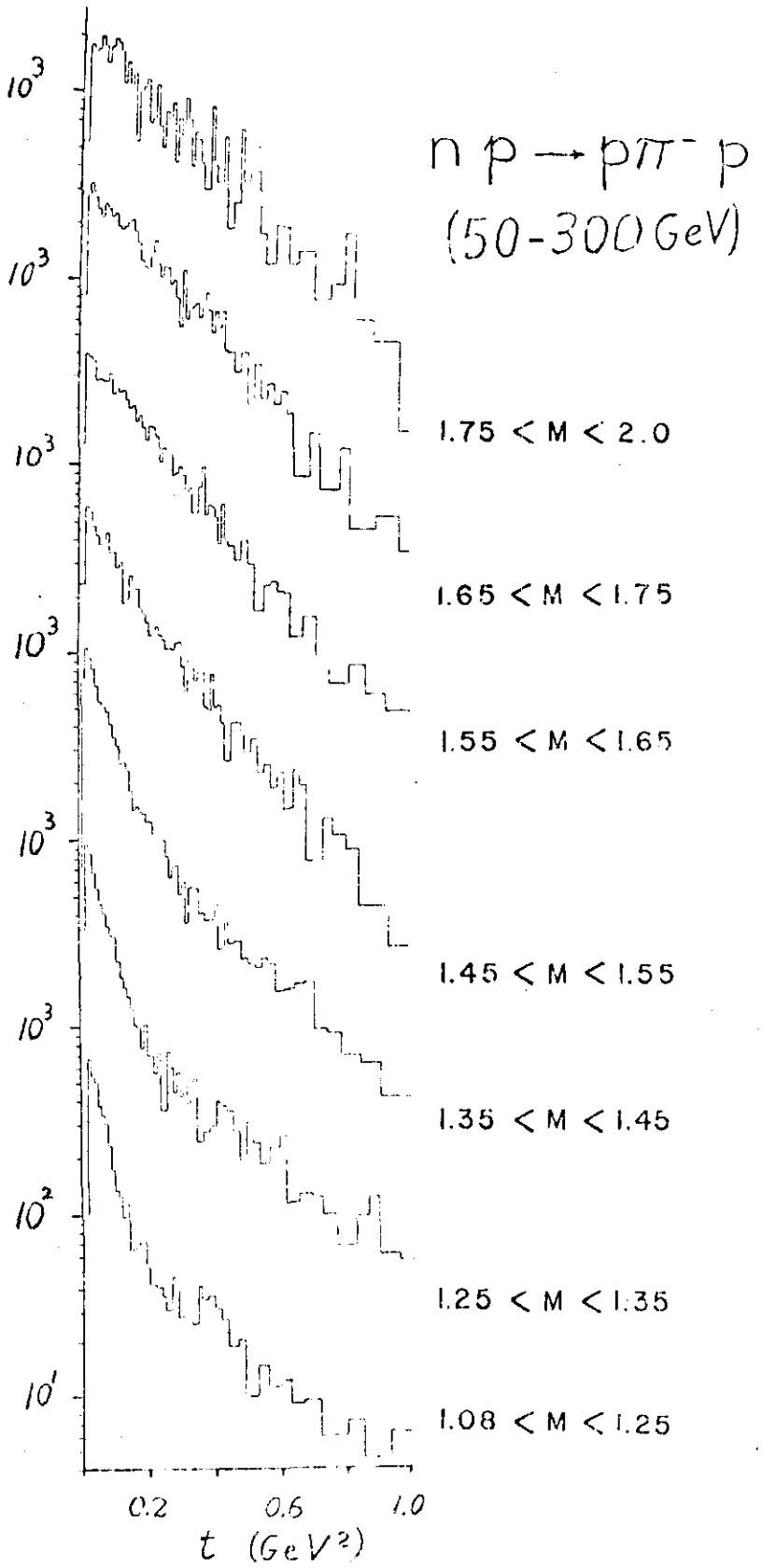

Fig. 9. Momentum transfer distributions for forward-produced $p\pi^-$ systems as a function of $p\pi^-$ mass.

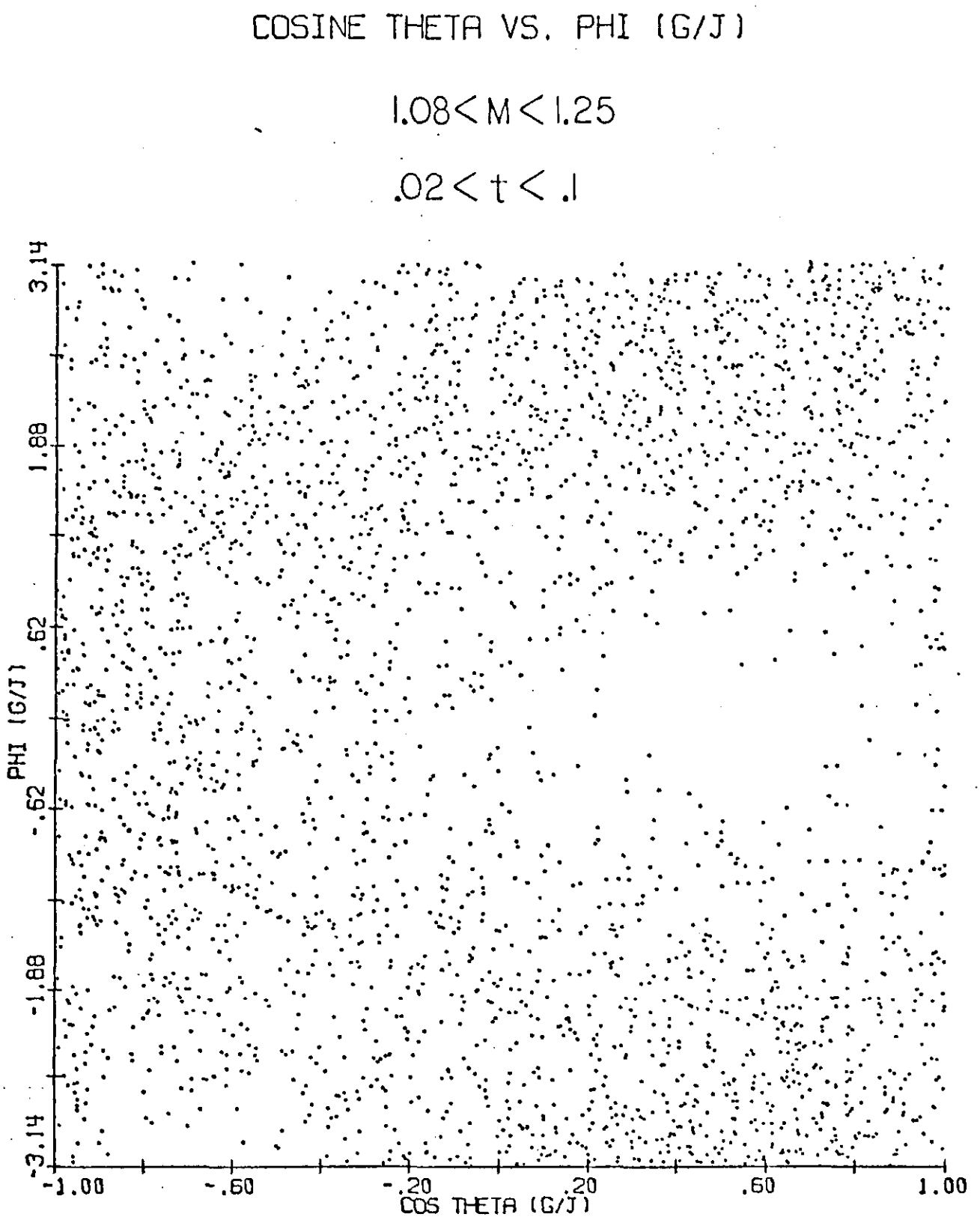

Fig. 10. Correlation between the cos θ and φ of the forward proton in the Gottfried-Jackson frame.

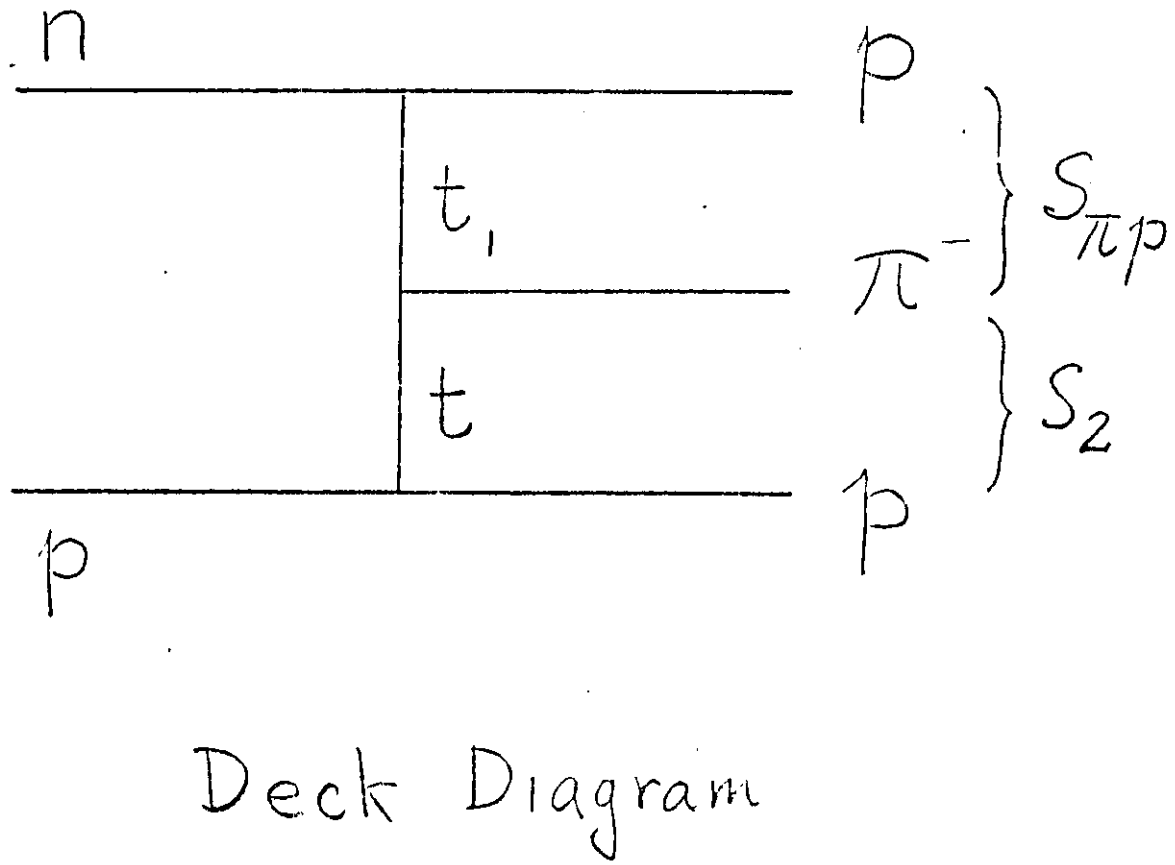

Fig. 11. The simple π-exchange Deck diagram for reaction (1).

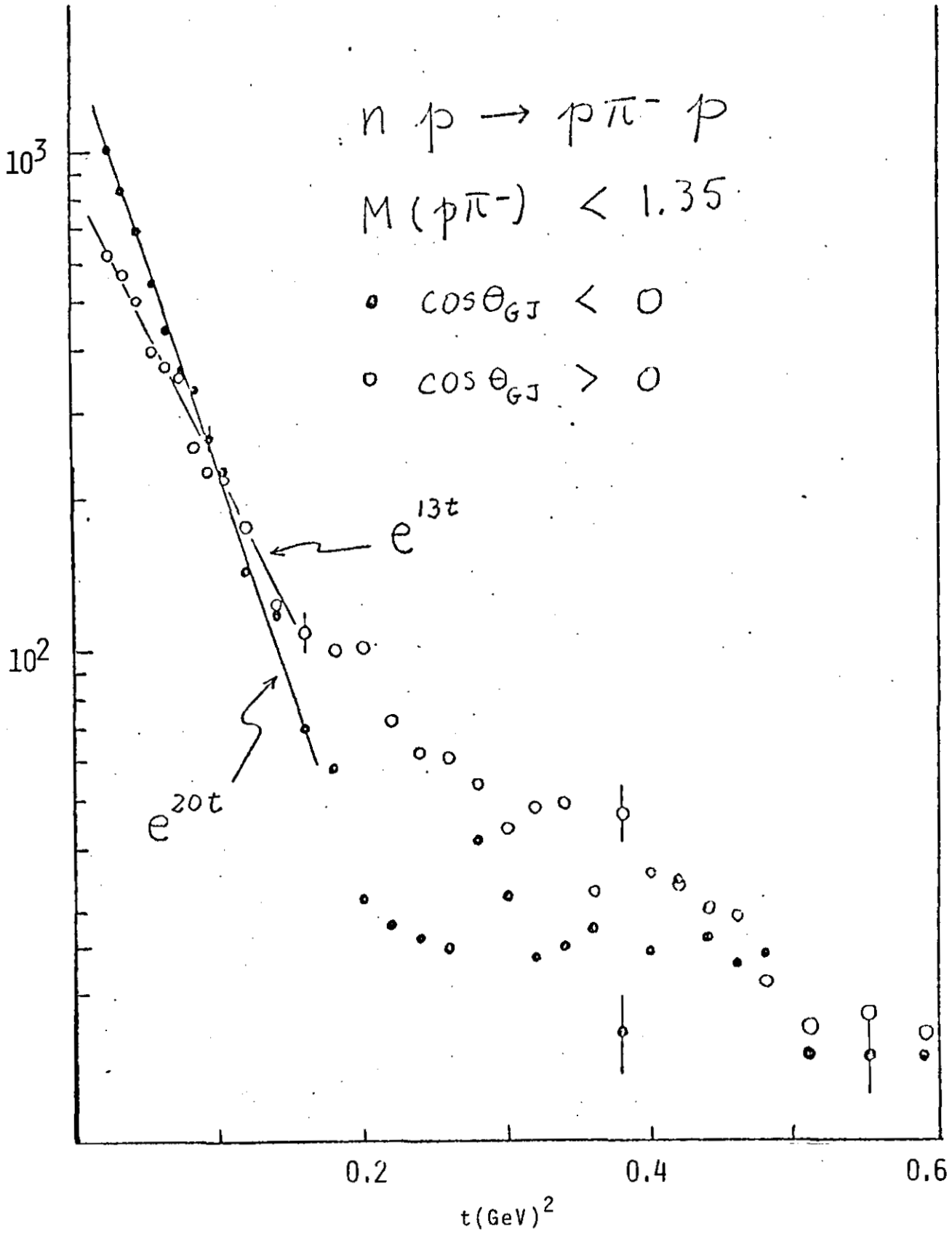

Fig. 12. The t-dependence on cosθ in the Gottfried-Jackson frame.

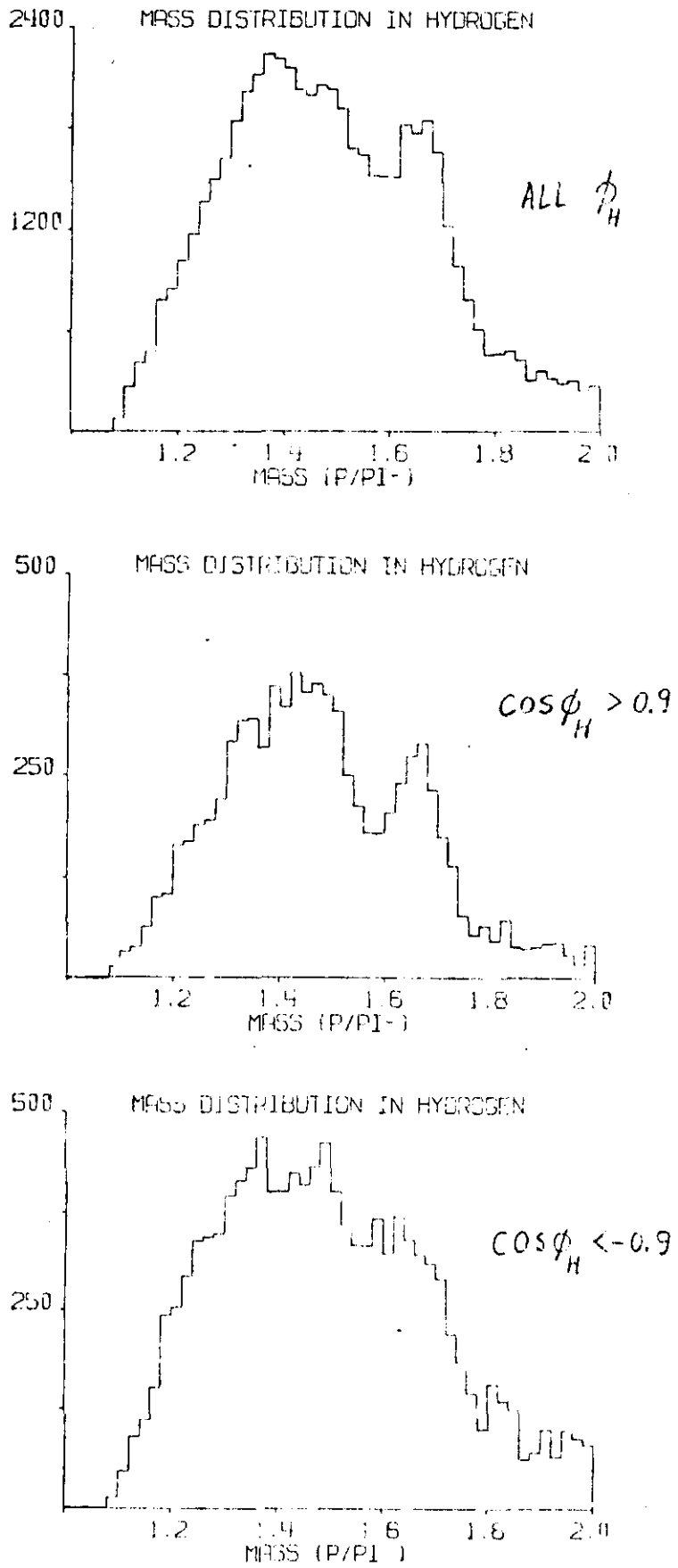

Fig. 13. Mass spectra for two regions of ϕ_H of the forward proton in the s-channel helicity frame. The Deck contribution is expected to dominate $\cos\phi_H < -0.9$.

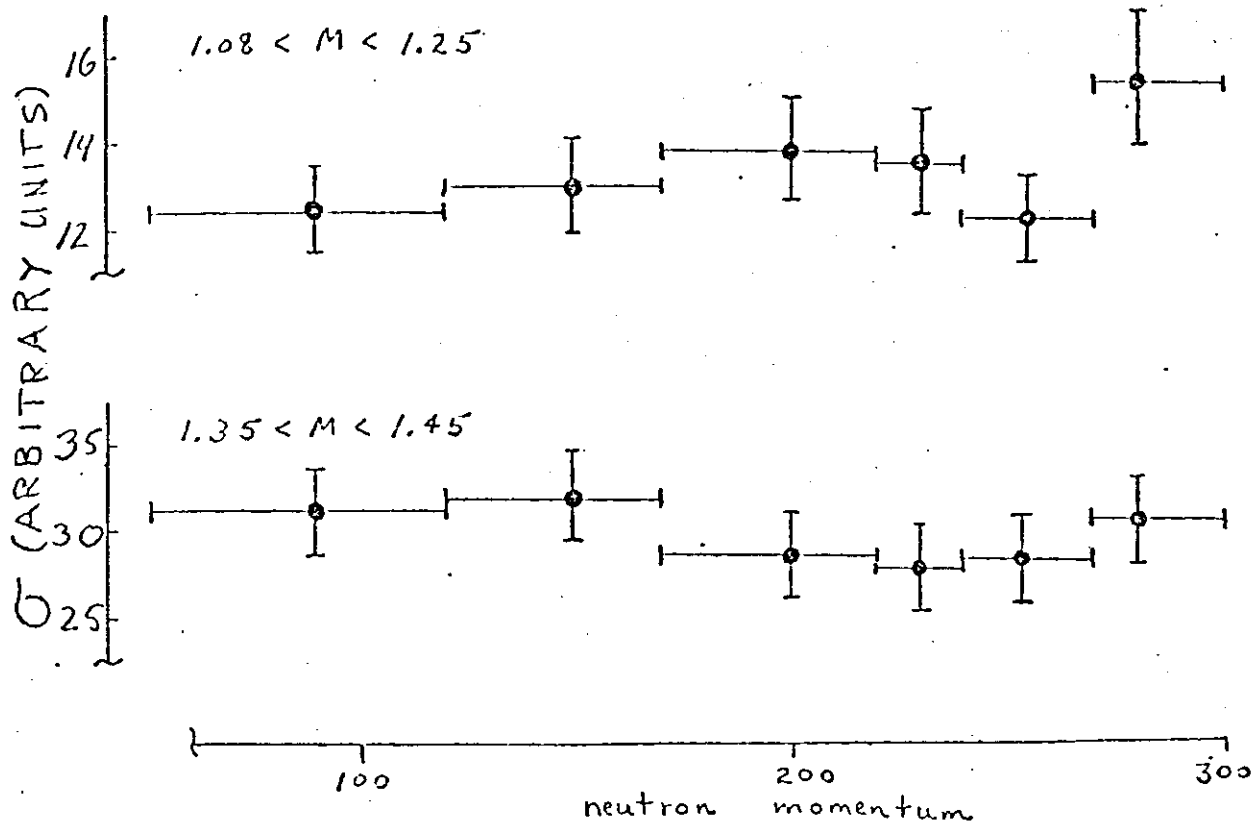

Fig. 14. Energy dependence of the cross section for neutron dissociation off a hydrogen target. The data have been integrated over t.

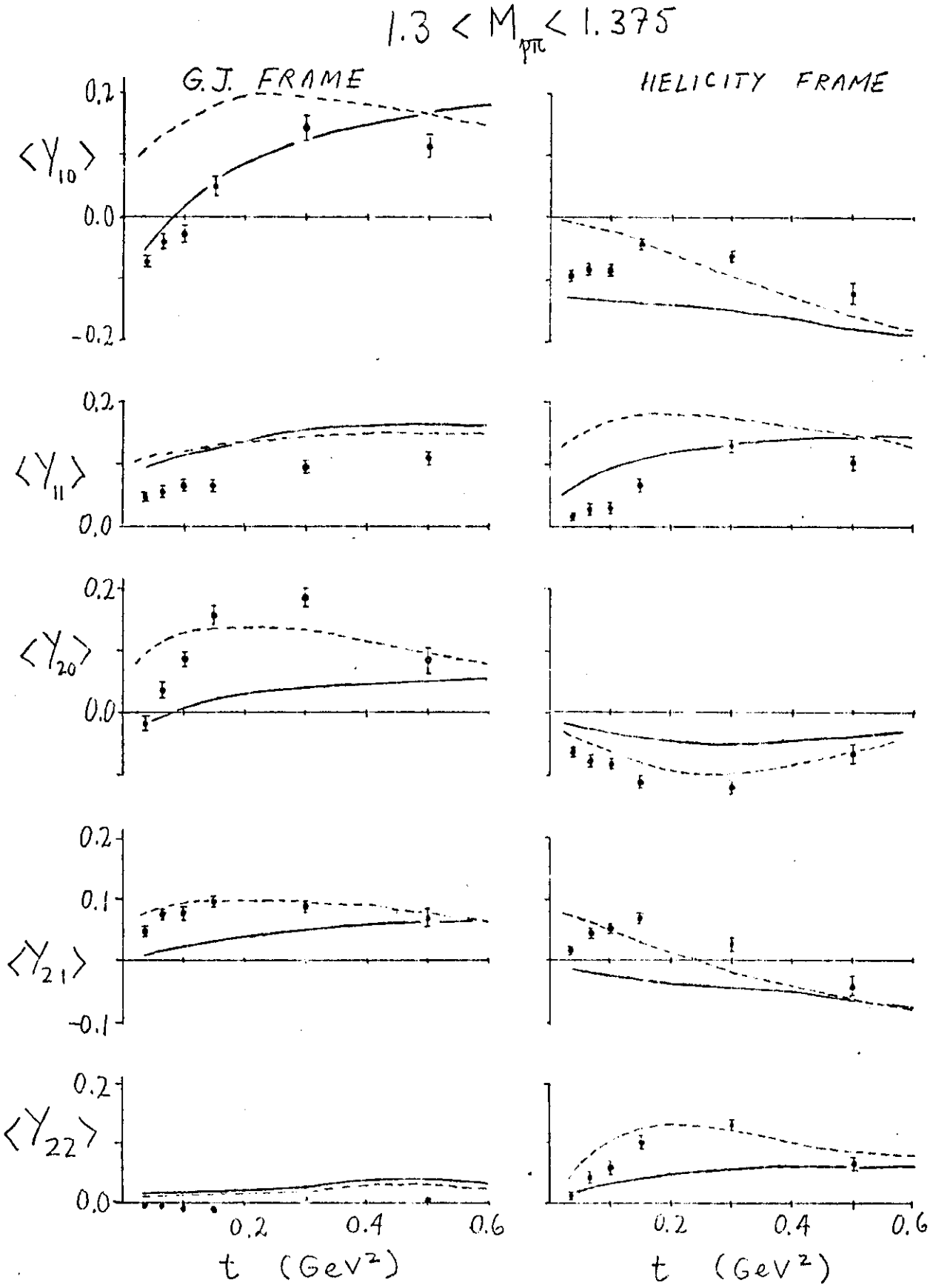

Fig. 15. The average $\langle Y_{\ell m}(\theta,\phi)\rangle$ moments as a function of $|t|$ for the $p\pi^-$ mass interval 1.300-1.375 GeV. The solid curves are predictions of equation (2). The dashed curves correspond to equation (2) but without the $(-t_1\, e^{2(t_1-\mu^2)})$ factor in front of the expression. The latter can be thought of as a Deck model with additional absorption.

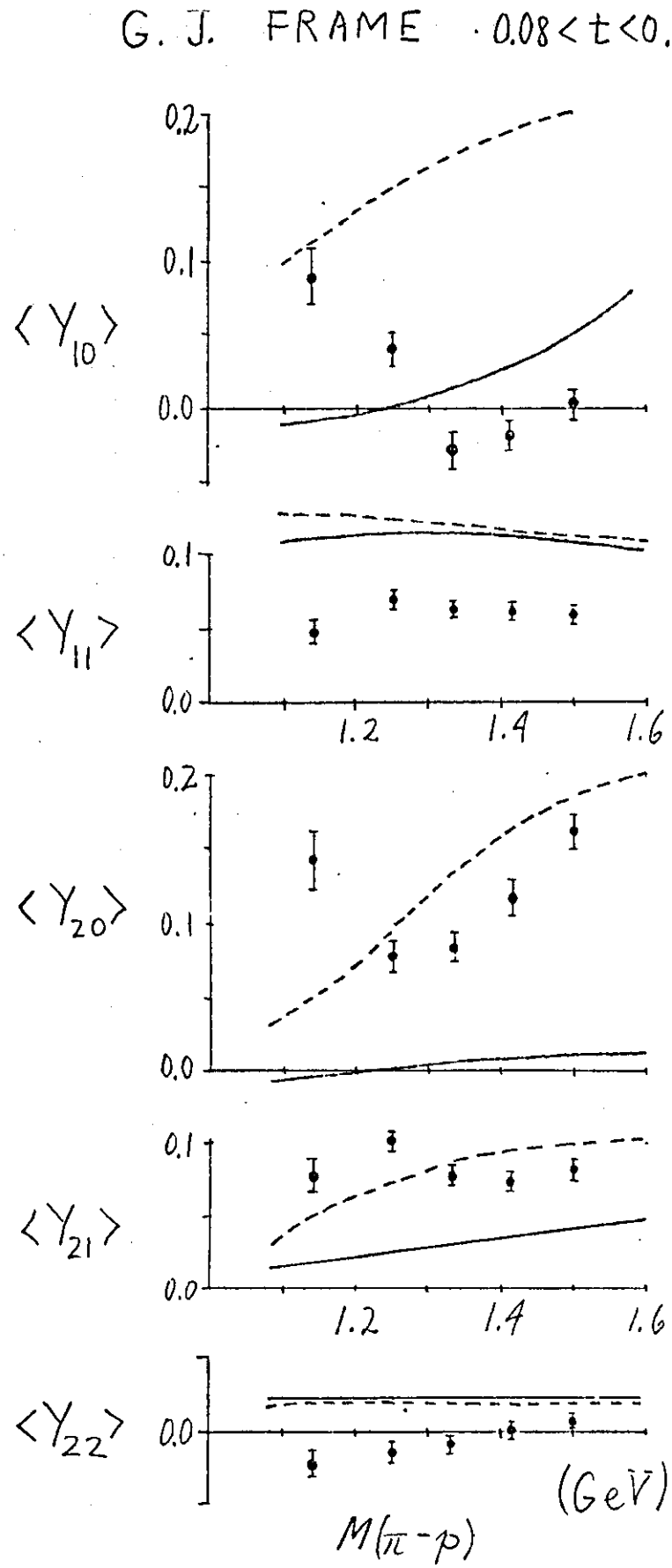

Fig. 16. The low order $\langle Y_{\ell m}(\theta,\phi)\rangle$ moments as a function of $p\pi^-$ mass for the $|t|$ interval 0.08 to 0.12 GeV^2. The solid curves are predictions of equation (2). The dashed curves correspond to equation (2) but without the $(-t_1\, e^{2(t_1-\mu^2)})$ factor in front of the expression. The latter can be thought of as a Deck model with additional absorption.

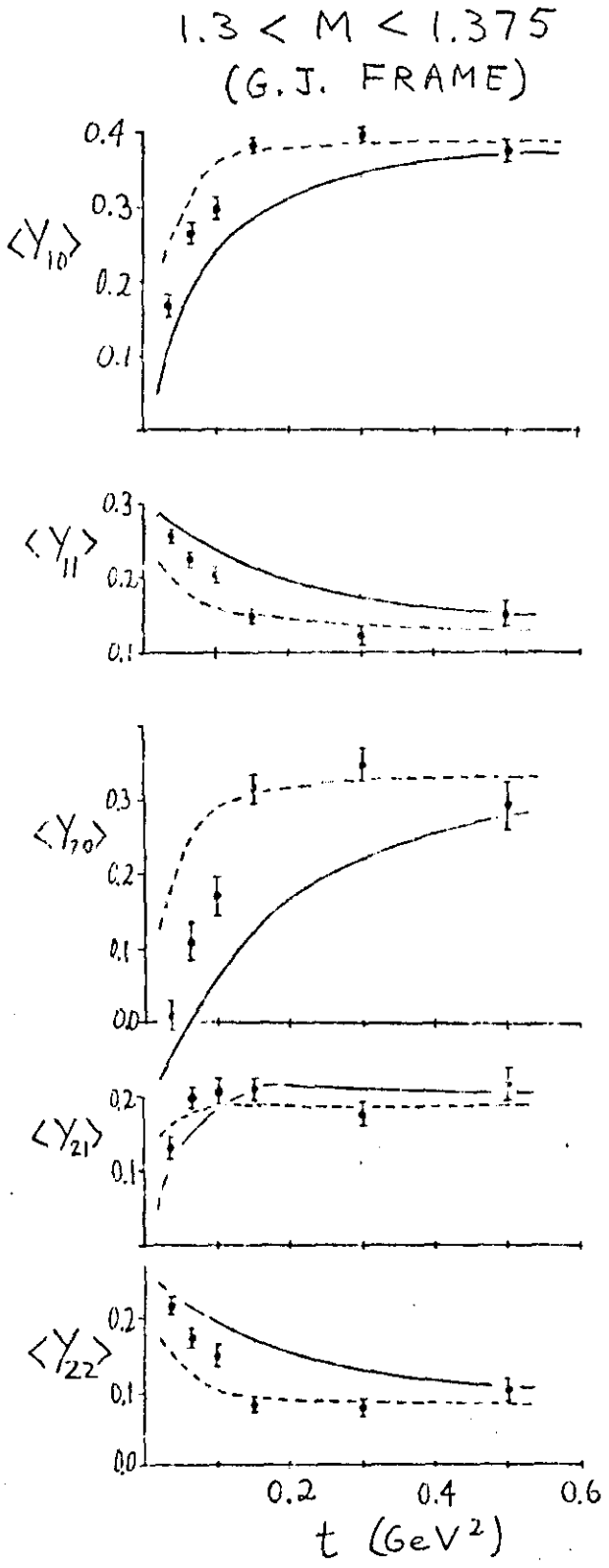

Fig. 17. The average $\langle Y_{\ell m}(\theta,\phi)\rangle$ moments as a function of $|t|$ for the $p\pi$ mass interval 1.300-1.375 GeV for $\cos\phi_H < -0.9$. The solid curves are predictions of equation (2). The dashed curves correspond to equation (2) but without the $(-t_1 e^{2(t_1-\mu^2)})$ factor in front of the expression. The latter can be thought of as a Deck model with additional absorption.

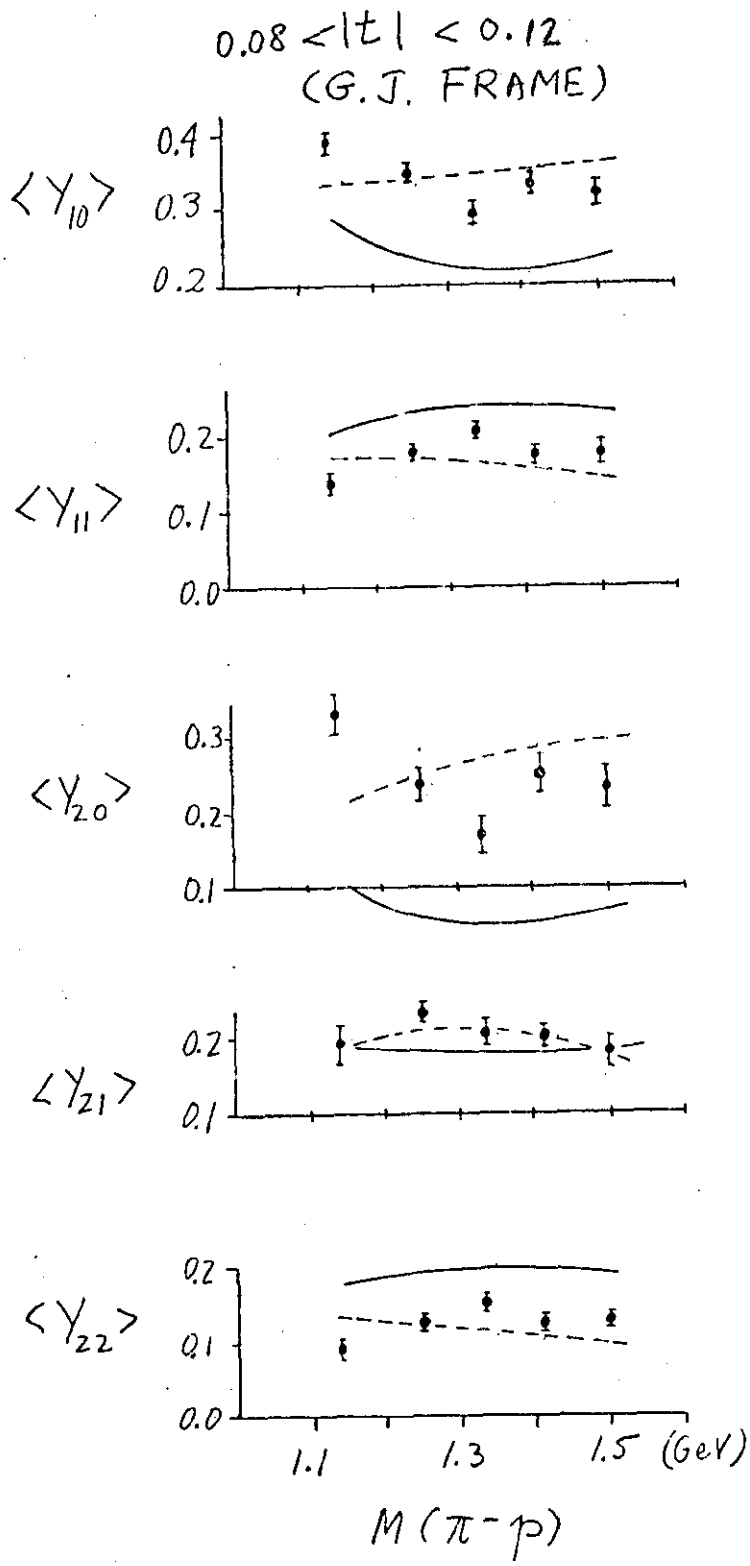

Fig. 18. The low order $\langle Y_{\ell m}(\theta,\phi)\rangle$ moments as a function of $p\pi^-$ mass for the $|t|$ interval 0.08 to 0.12 GeV^2 for $\cos\phi_H < -0.9$. The solid curves are predictions of equation (2). The dashed curves correspond to equation (2) but without the $(-t_1 e^{2(t_1-\mu^2)})$ factor in front of the expression. The latter can be thought of as a Deck model with additional absorption.

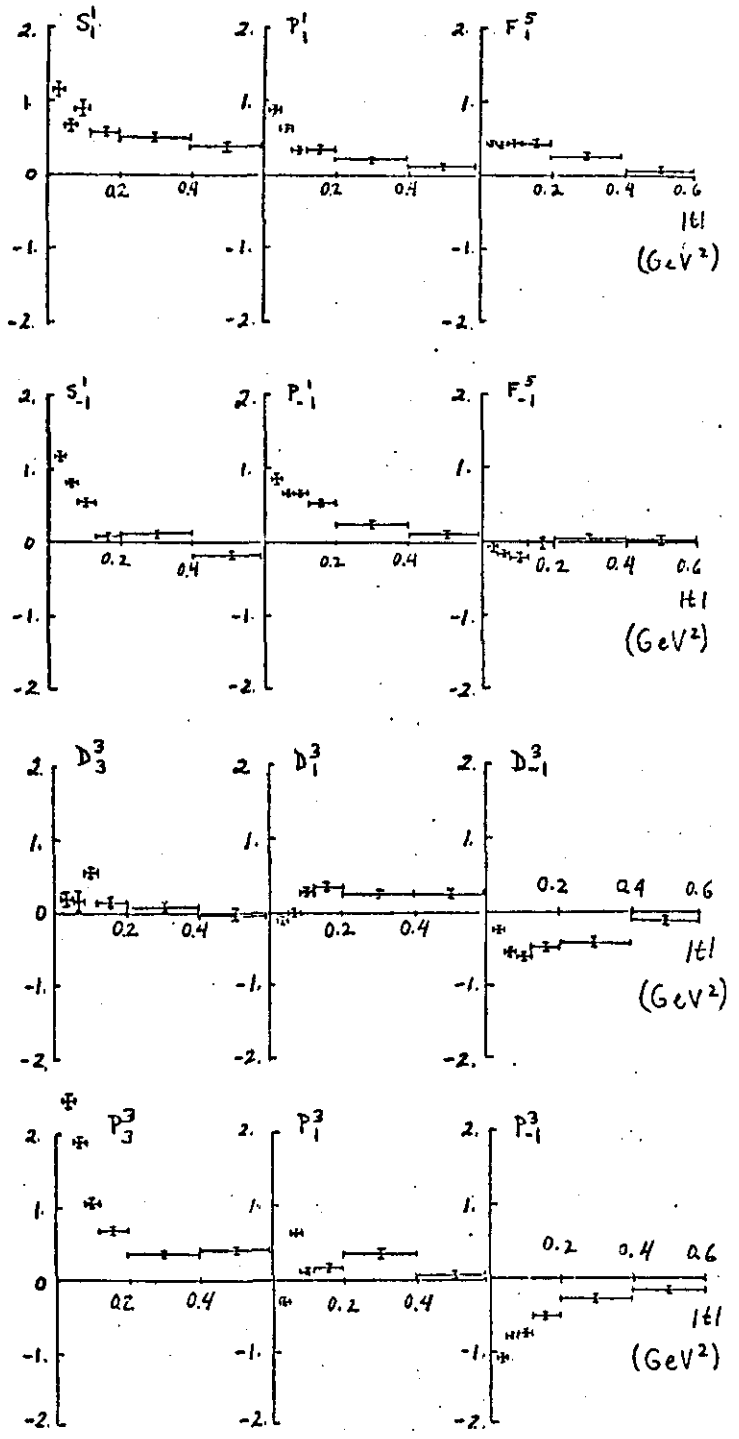

Fig. 19. Preliminary t-channel helicity amplitudes for the $p\pi^-$ mass range 1.3-1.375 GeV. The amplitudes are specified through the orbital wave (L), the total spin (J), and the helicity flip ($\Delta\lambda$) as $L^{2J}_{2\Delta\lambda+1}$. There is an ambiguity in the overall sign of the amplitudes. There is also an overall ambiguity in the relative parity of all even and odd states, e.g., the amplitudes labeled S^1, D^3, F^5 can be relabeled respectively as P^1, P^3, D^5 and vice versa.